Available online at www.sciencedirect.com
SCIENCE DIRECT
Journal of Molecular Catalysis A: Chemical 247 (2006) 88–98
JOURNAL OF MOLECULAR CATALYSIS A: CHEMICAL
www.elsevier.com/locate/molcata

Routes of formation and composition of NO_x complexes adsorbed on palladium-promoted tungstated zirconia

Margarita Kantcheva *, Ilknur Cayirtepe

Laboratory for Advanced Functional Materials, Department of Chemistry, Bilkent University, 06800 Bilkent, Ankara, Turkey

Received 21 September 2005; received in revised form 14 November 2005; accepted 16 November 2005
Available online 27 December 2005

Abstract

Surface species obtained during the adsorption of NO and NO/O_2 coadsorption at room temperature on Pd-free (WZ) and Pd-promoted tungstated zirconia (Pd/WZ) are identified by means of in situ FT-IR spectroscopy. The WZ and Pd/WZ samples have a tetragonal structure and contain randomly distributed mesoporous phase. Dispersed palladium(II) species are present in two different environments: (i) Pd^{2+} ions, which have only Zr^{4+} ions in their second coordination sphere and (ii) Pd^{2+} ions, which are linked to both zirconium and tungsten ions via oxygen bridges. On the Pd/WZ sample, NO undergoes oxidation to various NO_x species depending on the temperature. The compounds formed at room-temperature oxidation are adsorbed N_2O_3 and products of its self-ionization, NO^+ and NO_2^-. In this process W(VI) is involved, being reduced to W(IV). At high temperature N_2O_3 decomposes, restoring the W=O species. Under these conditions, NO undergoes oxidation to NO_2 by the Pd(II) ions, which are reduced to Pd(I). The nitrosyls of Pd(I) display high thermal stability and do not disappear upon evacuation at 623 K. During NO/O_2 coadsorption on the Pd/WZ catalyst at room temperature, the amounts of surface nitrates and NO_2/N_2O_4 formed in the gas phase are significantly lower than those observed under identical conditions in the presence of tungstated zirconia. It is concluded that promotion of tungstated zirconia with palladium(II) suppresses the oxidation of NO by molecular oxygen at room temperature due to the elimination of acidic protons involved in the process.

Keywords: NO adsorption; NO/O_2 coadsorption; NO_x adsorbed species; FT-IR spectroscopy; WO_3–ZrO_2; Pd/WO_3–ZrO_2

1. Introduction

Reduction of NO with CH_4 in the presence of oxygen (CH_4-SCR) is an attractive strategy for control of the exhaust from gas engines or turbines fueled with natural gas. Since the first report of Li and Armor [1] on Co-exchanged ZSM-5 catalysts, various zeolites containing transition and non-transition metals have been shown to be active in this reaction [2]. Palladium-exchanged H-ZSM5 and H-Mor catalysts are more attractive because they appear to be less sensitive to steam [3–7]. Nishizaka and Misono [8,9] first reported a high activity of Pd-exchanged H-ZSM-5 catalysts and indicated the direct involvement of protonic acid sites in both palladium dispersion and the mechanism of the CH_4-SCR of NO. Nowadays, it is widely accepted that the Brønsted acid sites of the zeolite are needed to keep palladium(II) highly dispersed and active [4,5,10–20] although the structure of the palladium species (isolated Pd^{2+} ions [10–15] versus highly dispersed PdO [16–20]) is still matter of discussion.

The use of zeolite-based catalysts for the CH_4-SCR of NO presents important drawbacks due to their low thermal stability and deactivation by water or SO_2. It has been shown that simple oxides with strong acidity, such as sulfated and tungstated zirconia, possess the ability to stabilize highly dispersed Pd(II) species analogous to the acidic zeolites [11,12,21–23]. Low-loading palladium catalysts supported on sulfated and tungstated zirconia exhibit catalytic properties in the CH_4-SCR of NO under dry conditions comparable to those of zeolitic catalysts and they show improved selectivity in the presence of H_2O and SO_2 [21–24].

Tungstated zirconia is thermally stable [25] and emerges as a good candidate for the replacement of zeolitic materials.

* Corresponding author. Tel.: +90 312 2902451; fax: +90 312 2664579.
E-mail address: margi@fen.bilkent.edu.tr (M. Kantcheva).

1381-1169/$ – see front matter © 2005 Elsevier B.V. All rights reserved.
doi:10.1016/j.molcata.2005.11.022

Maximum activity in the CH_4-SCR of NO is observed on zirconia catalysts containing up to 16–20 wt.% WO_3 and 0.1–0.17 wt.% Pd [21–24]. Tungstated zirconia is usually prepared by impregnation of hydrated zirconia with ammonium metatungstate, followed by calcination in the 873–1100 K range [25–29]. High density of strong acid sites can also be achieved by simultaneous coprecipitation with ammonia from solutions containing zirconium oxychloride and ammonium metatungstate [30].

Dispersed palladium species on tungstated zirconia have been identified by the appearance of two bands at 1868 and 1821 cm^{-1} in the IR spectra of adsorbed NO [22,23]. Similar bands have been observed on Pd-H-ZSM-5 and Pd-H-Mor and have been attributed to nitrosyls formed on isolated Pd^{2+} ions [3,5,16,17]. Other authors [31] have concluded, based on low-temperature CO adsorption, that the oxidation state of palladium deposited on tungstated zirconia is +3.

Since the dispersion of Pd(II) is favored by non-microporous materials [12], in this study we used Pd-free and Pd-promoted tungstated zirconia containing mesoporous phase. By means of in situ FT-IR spectroscopy we have identified the surface species, obtained during the adsorption of NO and NO/O_2 coadsorption on these materials. The samples have been characterized by XRD and DR-UV–vis spectroscopy. The localization of the Pd^{2+} species on the surface of tungstated zirconia has been studied by room-temperature adsorption of CO. The interaction of the surface NO_x complexes with methane can throw a light about the potentials of Pd-promoted tungstated zirconia containing mesoporous phase as a catalyst for the reduction of NO and the mechanism of the reaction. The results of this study will be reported separately.

2. Experimental

2.1. Sample preparation

Tungstated zirconia (notation WZ) was prepared by coprecipitation of aqueous solutions of $ZrOCl_2{\cdot}8H_2O$ (Merck) and ammonium metatungstate (Aldrich) with ammonia using polyvinyl alcohol (Aldrich) as a template according to a procedure described in detail in the literature [32]. The gel obtained was dried at 473 K for 24 h in air. The dried material was heated for 2 h at 673 and 923 K in an inert atmosphere (carbonization steps) followed by calcination at 773 K for 5 h. After fusion with $KHSO_4$ and dissolution in deionized water, the tungsten content was determined spectrophotometrically at $\lambda = 402$ nm using $TiCl_3$, $SnCl_2$ and NH_4SCN as chromogenic agents [33,34]. The WZ sample contained 18.6 wt.% WO_3.

The zirconia was synthesized by the same method [32], without the addition of ammonium metatungstate solution. The final carbonization temperature was 873 K. After that the material was calcined at 773 K for 5 h.

Palladium-promoted tungstated zirconia was prepared impregnating the WZ sample with a solution of $Pd(NO_3)_2{\cdot}2H_2O$ (Merck-Schuchardt) ensuring 0.1 wt.% of nominal palladium content. The sample was dried and calcined at 773 K for 5 h. For this sample the notation Pd/WZ is used.

The physico-chemical characteristics of the materials are summarized in Table 1.

2.2. Surface area measurements, X-ray diffraction and DR-UV–vis spectroscopy

The BET surface areas of the samples (dehydrated at 523 K) were measured by nitrogen adsorption at 77 K using a Monosorp apparatus from Quantachrome. XRD analysis was performed on a Rigaku Miniflex diffractometer with Ni-filtered Cu Kα radiation under ambient conditions. Crystallite sizes were calculated from the peak broadening of principal peaks with the Scherrer formula [36]. DR-UV–vis spectra were obtained under ambient conditions with a fiber optic spectrometer AvaSpec-2048 (Avantes) using WS-2 as a reference.

2.3. FT-IR spectroscopy

The FT-IR spectra were recorded on a Bomem MB 102 FT-IR spectrometer equipped with a liquid-nitrogen cooled MCT detector at a resolution of 4 cm^{-1} (128 scans). The self-supporting discs were activated in the IR cell by heating for 1 h in a vacuum at 773 K, and in oxygen (13.3 kPa, passed through a trap cooled in liquid nitrogen) at the same temperature, followed by evacuation for 1 h at 773 K. A specially designed transmission IR cell (Xenonum Scientific, USA) equipped with BaF_2 windows allowed recording of the spectra at elevated temperatures. The sample holder of the cell can be moved up and down relative to the light beam, giving the possibility of recording the gas phase spectrum. All of the FT-IR spectra presented (except those in Fig. 3A) were obtained by subtracting the spectra of the activated samples from the spectra recorded.

The CO (99.95%, BOC) used was passed through a trap cooled by liquid nitrogen before admission to the IR cell. The purity of the NO gas was 99.9% (Air Products).

Table 1
Physico-chemical characteristics of the samples

Sample	BET surface area (m^2/g)	WO_3[a] (wt.%)	Pd[b] (wt.%)	WO_3 (nm^2)	WO_3 coverage[c] (monolayer)
ZrO_2	96	–	–	–	
WZ	153	18.6	–	2.6	0.5
Pd/WZ	145	18.6	0.1	2.7	0.5

[a] Analytical content.
[b] Nominal content.
[c] Estimated by using the maximum packing density of planar WO_3 species of 0.21 g WO_3/100 m^2 [35].

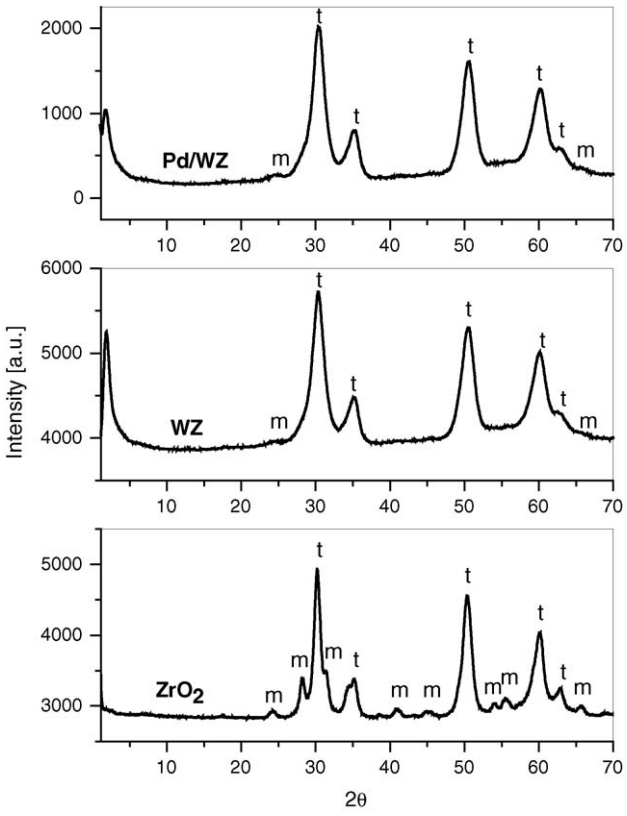

Fig. 1. Powder X-ray diffraction patterns of the calcined samples ZrO_2, WZ and Pd/WZ (m: monoclinic; t: tetragonal).

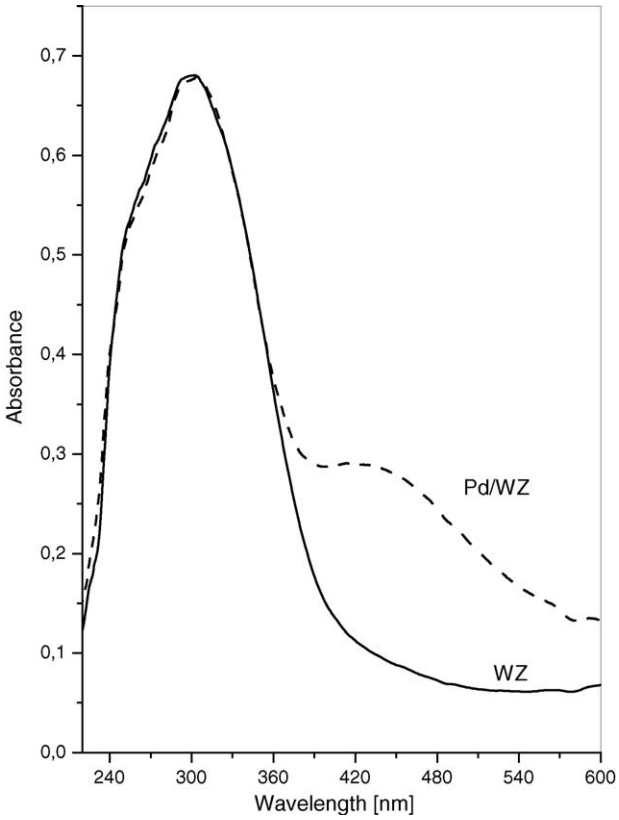

Fig. 2. UV–vis diffuse reflectance spectra of the calcined samples.

3. Results and discussion

3.1. Structural characterization of the samples

Fig. 1 shows the XRD patterns of the catalysts studied. The zirconia sample is a mixture of tetragonal and monoclinic phases. The stable crystalline form of ZrO_2 is monoclinic. However, the presence of residual carbonates (see below) leads to stabilization of a tetragonal phase. For this sample no mesoporous phase is detected. The average crystallite size is 7.7 nm. The WZ and Pd/WZ samples are predominantly tetragonal and contain a randomly distributed mesoporous phase, which is evident by the peak at $2\theta = 1.8^\circ$ [37]. This peak became lower in intensity and somewhat broader after the introduction of palladium indicating an increase in the pore size distribution relative to the WZ sample. The average crystallite size for both WZ and Pd/WZ samples is 4.9 nm. The mesopores collapse after calcination at 973 K.

The DR-UV–vis spectra obtained for tungstated zirconia and Pd-containing sample are shown in Fig. 2. The absorption spectrum of tungstated zirconia exhibits a strong band at 300 nm attributed to charge-transfer transitions in the W–O–W units [26]. Using the approach of Iglesia et al. [26,27], the width of the band gap, E_0, determined from a linear extrapolation to zero absorption in a plot of $(\alpha h\nu)^2$ versus $h\nu$ (α, absorbance; $h\nu$, photon energy) has a value of 3.38 eV. This value is similar to that of ammonium metatungstate and reveals the presence of polymeric tungstate domains of intermediate size [23,25–28].

Incorporation of palladium does not modify the spectrum of tungstated zirconia in the region of charge transfer transitions (Fig. 2), most probably because this absorption originates from the bulk phase of the sample. The band at 450 nm in the spectrum of the Pd/WZ sample is attributed to the d–d transition of either isolated Pd^{2+} ions linked to surface oxygen atoms of the support, or small $Pd(O)_n^{2+}$ entities [38]. Shimizu et al. [39] observed a similar band at 460–480 nm in the absorption spectrum of Pd-H-Mor. This band was attributed to d–d transitions of isolated Pd^{2+} ions coordinated to the cation exchange sites of the zeolite. It can be concluded that tungstated zironia prepared by coprecipitation is able to stabilize dispersed palladium(II) in a manner similar to the acidic zeolites.

3.2. FT-IR spectra of the activated samples and adsorption of CO

Fig. 3A shows the FT-IR spectra of the activated samples. The spectrum of ZrO_2 in the OH-stretching region displays a pair of bands at 3770 and 3745 cm^{-1}, strong absorption at 3665 cm^{-1} and a broad band between 3500 and 3000 cm^{-1}. According to the literature [40], the band at 3770 cm^{-1} is attributed to terminal OH groups due to monoclinic zirconia. The band at 3745 cm^{-1} arises from bibridged OH groups of tetragonal zirconia. The band at 3665 cm^{-1} is assigned to tribridged OH groups of monoclinic zirconia. The broad band between 3500 and 2750 cm^{-1} is attributed to H-bonded tribridged hydroxyls. The adsorption of CO (5.33 kPa) on this sample at room temperature does not

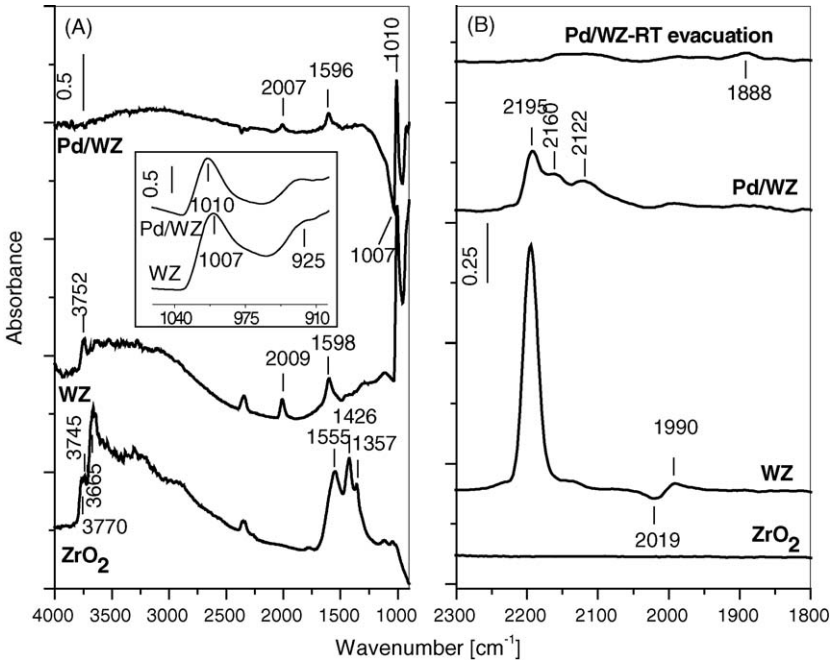

Fig. 3. (A) FT-IR spectra of the activated samples. (B) FT-IR spectra obtained upon adsorption of CO (5.33 kPa) for 45 min at room temperature. The spectra WZ and Pd/WZ are gas phase corrected.

lead to the formation of Zr^{4+}–CO species (Fig. 3B). The reason for this could be the presence of residual carbonates (strong bands in the 1600–1150 cm^{-1} region, Fig. 3A) which complete the coordination sphere of the exposed Zr^{4+} sites. The carbonate species appear during the calcination of the carbonized material and cannot be removed by a prolonged activation procedure.

The spectrum of the WZ sample (Fig. 3A) contains a sharp band at 3752 cm^{-1} corresponding to bibridged OH groups of tetragonal zirconia [40]. A broad band in the 3650–2500 cm^{-1} region reveals the presence of H-bonded hydroxyls. In the W=O stretching region (see also the inset in Fig. 3A) a single band at 1007 cm^{-1} with an overtone vibration [41] at 2009 cm^{-1} is detected. In the case of the WO_3–ZrO_2 system with similar WO_3 loading prepared by impregnation of hydrated zirconia with ammonium metatungstate, two bands at 1021 and 1014 cm^{-1} are reported [28,42,43]. These bands are assigned to two different oxo species. The presence of a single fundamental W=O band and a single overtone band indicates that the WZ sample contains only one type of W=O groups. It can be concluded that during the coprecipitation, better dispersion is achieved, leading to the formation of more uniform WO_x species. As proposed by Scheithhauer et al. [28,42], the unresolved absorption at 925 cm^{-1} can be assigned to W–O–Zr linkages.

CO does not form complexes with coordinatively unsaturated (cus) W^{6+} ions [28,42]. Thus the band at 2195 cm^{-1} observed upon adsorption of CO on the WZ sample (Fig. 3B) is attributed to Zr^{4+}–CO carbonyls. The modification of zirconia with WO_x species alters the basicity of the oxide ions leading to significant decrease in the amount of residual carbonates and appearance of coordinatively unsaturated Zr^{4+} sites upon activation. The adsorption of CO causes perturbation of the W=O stretching band. This is evident by the shift of the overtone vibration.

The spectrum of the Pd/WZ catalyst in the ν(OH) stretching region differs from that of the WZ support. There are no bands arising from isolated Zr^{4+}–OH groups and the absorption in the region of H-bonded hydroxyls is almost completely eroded. This indicates that during the deposition process, Pd^{2+} ions replace the protons of the surface hydroxyls. In addition, the incorporation of palladium causes both a shift in the position of the W=O fundamental band to 1010 cm^{-1}, and a decrease in its intensity. This behavior can be explained by assuming that some of the Pd^{2+} ions coordinate to the W=O species.

The spectrum of CO adsorbed on the Pd/WZ sample (Fig. 3B) shows that the amount of cus Zr^{4+} ions decreases considerably after the deposition of palladium. The bands at 2160 and 2122 cm^{-1} develop at the time of CO exposure and reach maximum intensity after 45 min. These bands do not disappear completely upon dynamic evacuation at room temperature. Since Pd(II) undergoes reduction in a CO atmosphere at room temperature [31], the bands at 2160 and 2122 cm^{-1} are attributed to Pd^{+}–CO carbonyls in two different environments. The weak feature at 1888 cm^{-1} detected upon evacuation corresponds to bridging CO adsorbed on metallic palladium [16]. It can be assumed that as a result of replacement of the protons of the isolated OH groups at 3752 cm^{-1} (Fig. 3A, spectrum WZ) there are Pd^{2+} ions linked to zirconium(IV) through oxygen atoms. These palladium species do not have tungstate groups in close proximity and upon CO adsorption give rise to the carbonyl band at 2122 cm^{-1}. Due to the charge-withdrawing WO_x species, the Pd^{2+} ions coordinated to the W=O groups possess increased electrophilicity and produce the carbonyl band at 2160 cm^{-1}. The location of the Pd^{2+} ions in the latter case can be described by the model shown in Scheme 1. The proposed structure accounts for both a lowering of the number of cus Zr^{4+}, and a decrease in

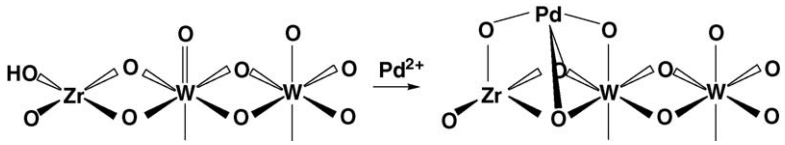

Scheme 1.

the intensity of the W=O band. Coordinatively unsaturated Zr^{4+} sites are created by dehydroxylation during the activation of the sample.

3.3. Adsorption of NO

The spectrum of NO (1.34 kPa) adsorbed on zirconia at room temperature is shown in Fig. 4A. The intense band at 1196 cm^{-1} is assigned to the ν(NO) stretching mode of anionic nitrosyl, NO^- [44]. Since Zr^{4+} ions are considered to be irreducible under these conditions, it is proposed that these species are formed by disproportionation of NO on surface O^{2-} sites:

$$4NO + 2O^{2-} \rightarrow NO_3^- + 3NO^- \quad (1)$$

According to the ν_3 spectral splitting [45], the NO_3^- species are of two types: bidentate nitrate at 1601 cm^{-1} corresponding to the ν(N=O) mode, and monodentate nitrate at 1495 cm^{-1} ($\nu_{as}(NO_2)$) and 1296 cm^{-1} ($\nu_s(NO_2)$) modes. Most probably the $\nu_{as}(NO_2)$ stretching vibration of the bidentate nitrate is covered by the strong NO^- band at 1196 cm^{-1}. This assumption is confirmed by the behavior of the bands upon evacuation (Fig. 4B): the absorption at 1196 cm^{-1} decreases in intensity, and the low-frequency component of the split ν_3 vibration of the bidentate nitrate is resolved at 1243 cm^{-1}. The spectrum of NO adsorbed on the ZrO_2 sample contains features that differ from those observed on monoclinic zirconia [44,46]. This could be associated with differences in the morphology, degree of hydroxylation and presence of impurities.

The adsorption of NO (1.34 kPa) on the WZ sample at room temperature produces a more complex spectrum than that of zirconia (Fig. 4A). Despite the presence of species that are common for both the WZ sample and tungstated zirconia obtained by impregnation of $Zr(OH)_4 \cdot xH_2O$ with ammonium metatungstate (19 wt.% of WO_3), the interpretation of the spectrum of adsorbed NO in this study differs from that proposed for the impregnated material [47]. The assignment of the bands takes into account their development with the time of NO exposure, behavior upon evacuation at room temperature and the fact that tungsten(VI) does not form nitrosyls [48–50]. All of the bands appear in the spectrum immediately after the introduction of NO to the IR cell except the absorption at 1950 cm^{-1}. They increase in intensity with the time of NO exposure except those at 2243 and 1215 cm^{-1}. The spectrum obtained after 30 min is shown in Fig. 4A. The sharp, intense band at 2243 cm^{-1} and the absorption at 1215 cm^{-1} correspond to adsorbed N_2O and belong to the ν(NN) and ν(NO) stretching vibrations, respectively [47]. The broad band at 2131 cm^{-1} is typical of adsorbed NO^+ species and

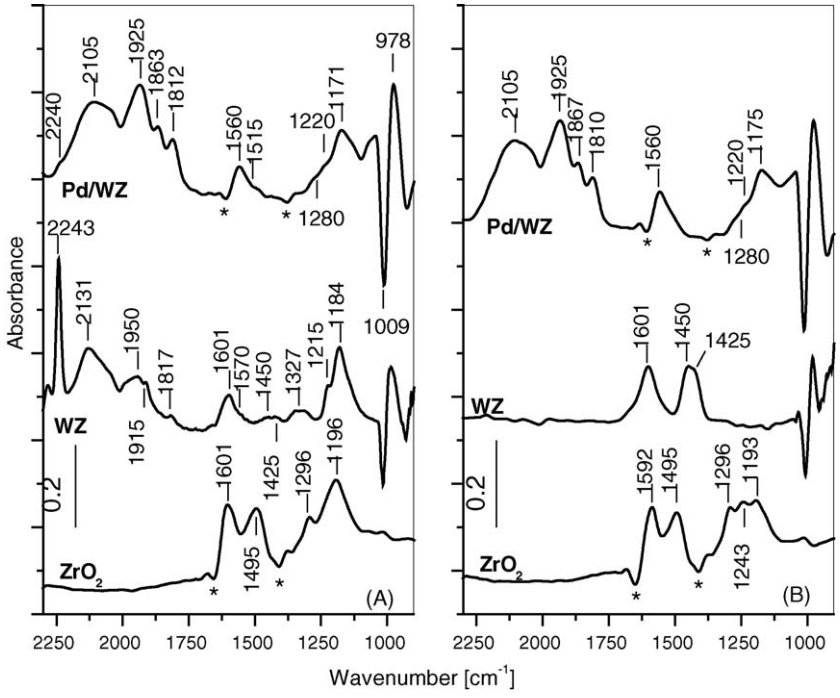

Fig. 4. (A) FT-IR spectra of NO (1.33 kPa) adsorbed for 30 min at room temperature on the samples studied. The gas phase spectra are subtracted. (B) After evacuation for 15 min at room temperature. The negative bands marked by asterisks are due to residual carbonates, which are removed by the NO_x species.

belongs to the ν(NO) mode [47]. The band at 1950 cm^{-1}, which is absent from the spectrum at the beginning of the process, is assigned to NO adsorbed on Zr^{4+} sites with increased electrophilicity caused by induction effect from adjacent electron-withdrawing NO_x species [47]. The shoulder at about 1915 cm^{-1} and the weak absorption centered at 1327 cm^{-1} are attributed to the ν(N=O) and $\nu_s(NO_2)$ modes of adsorbed N_2O_3, respectively [44,45,51]. The $\nu_{as}(NO_2)$ stretching vibration appears usually at 1590–1550 cm^{-1} [45] and overlaps with the band at 1601 cm^{-1}. The assignment of the latter absorption is proposed below. The weak band at 1817 cm^{-1} can be attributed to NO adsorbed on reduced tungsten species. According to the literature [49,50], W^{5+}–NO nitrosyls possess ν(NO) stretching vibrations at 1843–1856 cm^{-1}. These species disappear upon evacuation. In contrast, the W^{4+} ions form stable $W^{4+}(NO)_2$ dinitrosyls characterized by a pair of bands at 1765–1785 and 1691–1700 cm^{-1} [48–50]. Although the band at 1817 cm^{-1} disappears upon evacuation (Fig. 4B, spectrum WZ), it cannot be attributed to W^{5+}–NO species, because it is positioned below 1840 cm^{-1}. For this reason, we assign this band to the ν(NO) stretching mode of W^{4+}–NO nitrosyl that has NO_x^- species in its coordination sphere, i.e. to the complex ON–W^{4+}–NO_x^- (most probably $x=2$, see below). The electron-withdrawing NO_x^- species increase the electrophilicity of the W^{4+} ion. This causes decrease in the π contribution to the bond of adsorbed NO, i.e. weaker W^{4+}–NO bond. It is assumed that the W^{4+} ions appear in the following process:

$$2NO + W^{6+}{=}O^{2-} \rightarrow N_2O_3 + W^{4+} \quad (2)$$

The adsorbed N_2O_3 can undergo self-ionization according to the reaction [51]:

$$N_2O_3 \rightleftharpoons NO^+ + NO_2^- \quad (3)$$

The NO_2^- species formed in reaction (3) are identified as bidentate nitrito species characterized by the absorption at 1184 cm^{-1} due to the $\nu_s(NO_2)$ mode [45]. The $\nu_{as}(NO_2)$ mode most probably is superimposed on the band at 1215 cm^{-1}, which is assigned to the adsorbed N_2O. Under dynamic evacuation (Fig. 4B) the bidentate nitrito species disappear together with the adsorbed N_2O_3 and NO^+ ions. This confirms the occurrence of equilibrium (3), and supports the proposed assignment of the bands. In the spectrum taken under these conditions, the bands at 1605, 1450 and 1425 cm^{-1} show increased intensities (Fig. 4B). The latter two bands are attributed to ν(N=O) modes of two types of monodentate nitrito species [45]. The concomitant ν(NO) stretching vibrations fall in the 1100–1050 cm^{-1} region [45] and are covered by the strong ν(W=O) band due to the perturbed tungstate species. In order to explain the growth of the bands at 1605, 1450 and 1425 cm^{-1} observed upon dynamic evacuation, the following interaction between the adsorbed N_2O_3 and the surface hydroxyls is assumed:

$$N_2O_3 + 2OH^- \rightarrow H_2O + 2NO_2^- \quad (4)$$

The band at 1601 cm^{-1} is assigned to the $\delta(H_2O)$ mode of adsorbed water. This assignment is supported by the fact that in the OH-stretching region (not shown) in the presence of NO, a negative band develops at 3750 cm^{-1} (due to altered Zr^{4+}–OH groups) accompanied by a positive absorption in the 3500–3000 cm^{-1} region. The intensities of these bands increase with dynamic evacuation of NO.

Another possibility for formation of N_2O_3 is through disproportionation of NO with N_2O as a concomitant product [51]. This process does not require the presence of redox sites and if it takes place, adsorbed N_2O should appear also in the case of zirconia. Since this species was not detected on the latter sample (Fig. 4A), it is assumed that N_2O observed on the WZ is formed by a different process, e.g. adsorption of NO on oxygen vacancies [52].

The spectrum of NO (1.34 kPa) adsorbed on the Pd/WZ catalyst at room temperature displays features similar to those observed for the tungstated zirconia (Fig. 4). However, some differences should be noted:

1. In agreement with the literatures [3,5,16,17,22,23], the bands at 1863 and 1812 cm^{-1} are due to NO adsorbed on Pd(II) sites in two different environments. The intensities of the Pd^{2+}–NO bands do not change with the time of NO exposure. By analogy with the results of CO adsorption, it is proposed that the band at 1812 cm^{-1} represents NO adsorbed on Pd^{2+} sites, which have only Zr^{4+} ions in their second coordination sphere. The band at 1863 cm^{-1} is attributed to the ν(NO) stretching mode of NO adsorbed on Pd^{2+} ions with enhanced Lewis acidity due to an induction effect from adjacent WO_x species.
2. Most probably, the absorption at 1817 cm^{-1} assigned to the ν(NO) stretching mode of the mixed nitrosyl-nitrato complex of W^{4+} is covered by the stronger Pd^{2+}–NO nitrosyl bands and cannot be detected.
3. The N_2O_3 (ν(N=O) at 1925 cm^{-1}, $\nu_{as}(NO_2)$ at 1560 cm^{-1} and $\nu_s(NO_2)$ at 1280 cm^{-1}) and the bidentate nitrito species with $\nu_{as}(NO_2)$ and $\nu_s(NO_2)$ modes at 1220 and 1171–1175 cm^{-1}, respectively, resist evacuation. The stabilization of the adsorbed N_2O_3 on the surface of the Pd/WZ catalyst can be explained by the fact that this sample does not contain isolated OH groups (see Fig. 3A). This behavior confirms the occurrence of the process described by Eq. (4).

The spectra of the tungstated materials display negative bands at 1009 cm^{-1} and positive absorption at 978 cm^{-1} due to perturbation of the wolframyl groups. The gas phase spectra taken in the presence of the WZ and Pd/WZ samples do not contain bands attributable to N_2O_3. Most probably, N_2O_3 is present on the surface as condense phase, or its concentration in the gas phase is low and cannot be detected under the conditions of the existing path length of the IR cell.

Table 2 summarizes the assignments of the IR bands of the NO_x compounds obtained during the adsorption of NO at room temperature.

3.3.1. High-temperature adsorption of NO

Fig. 5A shows the spectrum of the Pd/WZ catalyst taken after adsorption of NO (1.34 kPa) for 15 min at room temperature

Table 2
Assignments of the FT-IR bands observed upon room-temperature adsorption of NO on the samples studied

Sample	NO_x species	Band position (cm^{-1})	Mode
ZrO_2	NO_3^- (bidentate)	1601, 1243	ν(N=O), $\nu_{as}(NO_2)$
	NO_3^- (monodentate)	1495, 1296	$\nu_{as}(NO_2)$, $\nu_s(NO_2)$
	NO^-	1196	ν(NO)
WZ	N_2O (ads.)	2243, 1215	ν(NN), ν(NO)
	NO^+	2131	ν(NO)
	ON–Zr^{4+}–NO_x	1950	ν(NO)
	N_2O_3 (ads.)	1915, 1517 1327	ν(N=O), $\nu_{as}(NO_2)$, $\nu_s(NO_2)$
	NO–W^{4+}–NO_2^-	1817	ν(NO)
	H_2O (ads.)	1605	$\delta(H_2O)$
	NO_2^- (monodentate nitrito, two types)	1450, 1425	ν(NO)
	NO_2^- (bidentate nitrito)	1184	$\nu_s(NO_2)$
Pd/WZ	N_2O (ads.)	2240	ν(NN)
	NO^+	2105	ν(NO)
	N_2O_3 (ads.)	1925, 1560, 1280	ν(N=O), $\nu_{as}(NO_2)$, $\nu_s(NO_2)$
	Pd^{2+}–NO (two types)	1863, 1812	ν(NO)
	NO_2^- (bidentate, nitrito)	1220, 1171	$\nu_{as}(NO_2)$, $\nu_s(NO_2)$

(spectrum a), followed by heating the closed IR cell for 15 min at 623 K (spectrum b). The latter treatment causes all of the NO_x species observed at room temperature to disappear. Consequently, the altered WO_x species are almost completely restored. This behavior can be explained by assuming that at high temperatures, reaction (2) shifts to the left. This assumption is supported by the fact that N_2O_3 is stable at low temperature [53].

The gas phase spectrum recorded at 623 K (Fig. 5B, spectrum b) contains NO_2 in addition to the NO. Some amount of N_2O is also detected. This was already present at room temperature (Fig. 5B, spectrum a). Based on this, the weak band at 1613 cm^{-1} in spectrum b (Fig. 5A) is attributed to adsorbed NO_3^- species. This experimental fact reveals that oxidation of NO has occurred. The strong perturbation in the region of the Pd^{2+}–NO nitrosyls suggests that in this process, the Pd^{2+} ions are involved. The weak bands at 1863 and 1816 cm^{-1} corresponding to the Pd^{2+}–NO nitrosyls have disappeared, and considerably stronger bands at 1837 and about 1790 cm^{-1} (shoulder) are detected instead. These two bands are assigned to the Pd^+–NO species [54], which originate from the Pd^{2+}–NO nitrosyls observed at room temperature. This assignment is justified by the fact that under the same experimental conditions, all of the NO_x

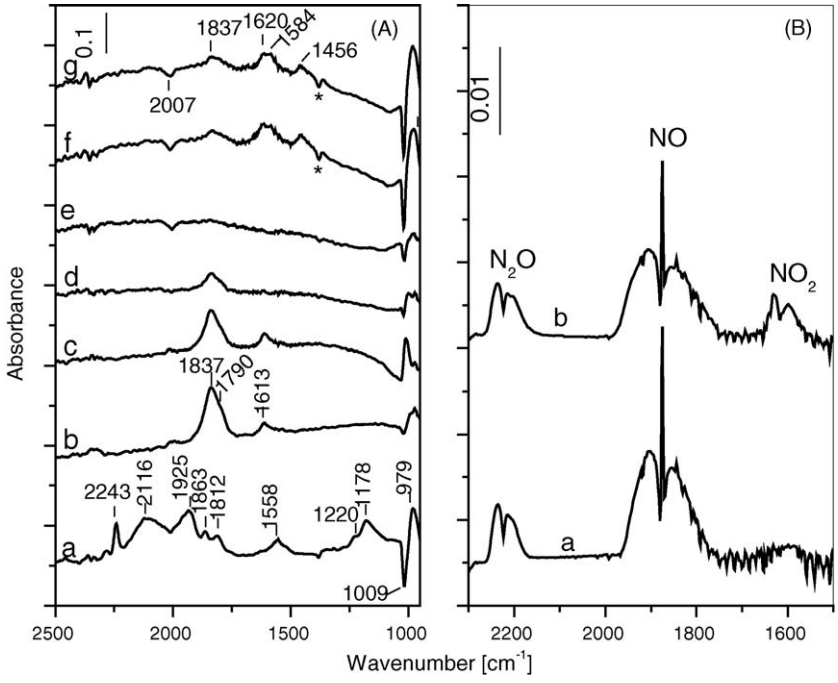

Fig. 5. (A) FT-IR spectra of the Pd/WZ sample taken after adsorption of NO (1.33 kPa) at room temperature for 15 min (a), after heating of the closed IR cell for 15 min at 623 K (b), and subsequent evacuation for 15 min at 623 K (c), then heating the closed IR cell for 15 min at 723 K (d), at 773 K (e) and after cooling down to room temperature (f) followed by evacuation for 15 min at room temperature (g). The gas phase spectra are subtracted. The negative bands marked by asterisks are due to residual carbonates, which are removed from the surface by the NO_x species formed. (B) Gas phase spectra recorded at room temperature (a) and 623 K (b).

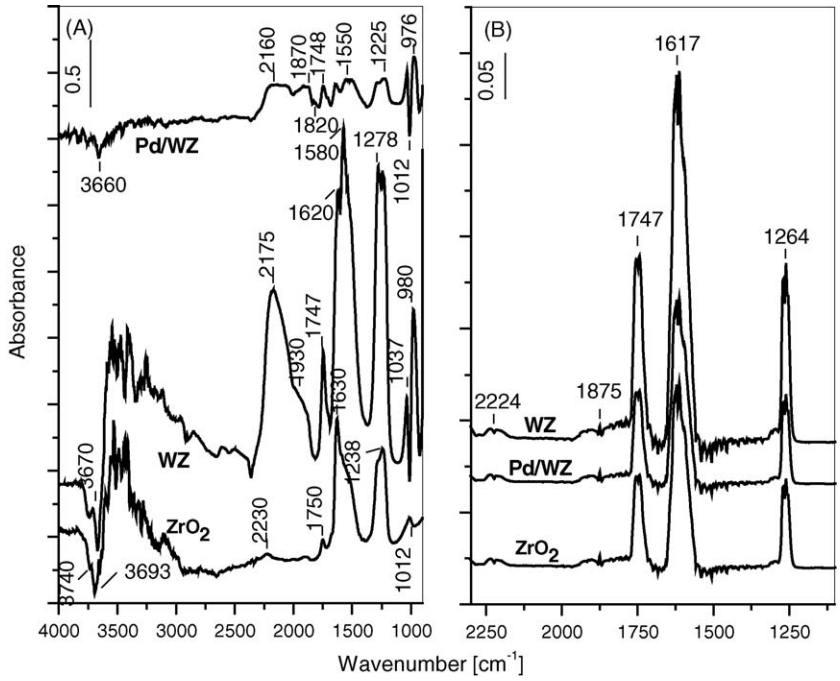

Fig. 6. (A) FT-IR spectra of NO (1.34 kPa) adsorbed at room temperature for 10 min (ZrO_2 and WZ samples) and 30 min (Pd/WZ sample), and after subsequent introduction of O_2 (2.66 kPa) for 30 min. The spectra are gas phase corrected. (B) Gas phase spectra recorded in the presence of WZ and Pd/WZ samples.

complexes formed on the WZ support by room-temperature adsorption of NO disappear. No absorption bands which can be attributed to nitrosyls of reduced tungsten species are detected.

The Pd^+–NO nitrosyls display high thermal stability and resist the evacuation at 623 K (Fig. 5A, spectrum c). Increasing the temperature of the closed IR cell to 723 K (Fig. 5A, spectrum d) leads to desorption of the nitrate species, and then at 773 K (Fig. 5A, spectrum e) to loss of NO adsorbed on the Pd^+ sites. Cooling to room temperature (Fig. 5A, spectra f and g) causes the reappearance of Pd^+–NO bands with reduced intensities relative to those in spectrum c. This indicates that additional oxidation of NO to NO_2 has occurred, leading to the formation of nitrate species at 1620, 1584 and 1456 cm^{-1}.

3.3.2. *Coadsorption of NO and O_2*

Fig. 6A shows the spectra of the samples studied after the adsorption of 1.34 kPa of NO and subsequent addition of 2.66 kPa of O_2 to the IR cell at room temperature. This causes significant changes in the spectra of preadsorbed NO. In the case of ZrO_2, the NO^- species disappear and the intensities of the nitrate bands with maxima at 1630, 1238 and 1012 cm^{-1} increase. The band at 1750 cm^{-1} reveals the presence of adsorbed N_2O_4 ([46], see Fig. 6B). The weak band at 2230 cm^{-1} which is detected also in the spectrum taken during the room-temperature evacuation (Fig. 7) is attributed to adsorbed NO^+ species [44–46]. The Zr–OH hydroxyls at 3740 and 3693 cm^{-1} are perturbed giving rise to positive absorption in the region of H-bonded OH groups. The gas phase spectrum obtained in the presence of zirconia contains bands due to N_2O_4 (ν_{as}(NO) at 1747 cm^{-1} and ν_s(NO) at 1264 cm^{-1}) and NO_2 ($\nu_{as}(NO_2)$ at 1617 cm^{-1}) [53]. The weak absorption at

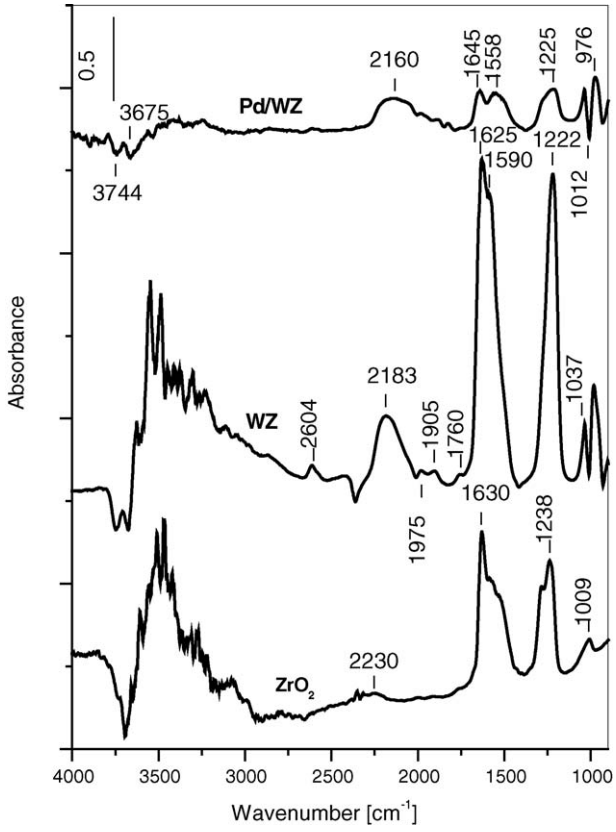

Fig. 7. FT-IR spectra obtained upon dynamic evacuation of pre-adsorbed NO_x species for 15 min (ZrO_2 and WZ) and 30 min (Pd/WZ) at ambient temperature. For the experimental conditions of NO/O_2 adsorption see Fig. 6.

2224 cm^{-1} belongs to the ν(NN) mode of N_2O, whereas that at 1876 cm^{-1} corresponds to the ν(NO) stretching of NO [53]. NO_2 and N_2O_4 are formed by the reaction of NO with O_2 in the gas phase ($2NO + O_2 = 2NO_2/N_2O_4$). The intensities of the bands of the gas phase spectrum taken in the presence of zirconia are identical to those of the spectrum of $NO + O_2$ obtained in absence of ZrO_2. This indicates that the ZrO_2 sample does not catalyze the oxidation of NO by molecular oxygen at room temperature. The adsorbed species resist room-temperature evacuation (Fig. 7).

It is known from the chemistry of NO_2 [55] that NO_2 disproportionates in basic solutions to nitrate and nitrite ions with formation of water. Similar process (Eq. (5)) has been proposed to take place upon interaction of NO_2 with oxides containing basic OH groups such as titania (anatase) [56–58] and monoclinic zirconia [44,46]:

$$2OH^- + 3NO_2(1.5N_2O_4) \rightarrow 2NO_3{}^- + NO + H_2O \quad (5)$$

The formation of water molecules has been confirmed by adsorption of NO_2 on deuterioxylated TiO_2 [56].

Another possibility for the formation of nitrate species is through self-ionization of NO_2 on surface Lewis acid–base pairs according to the reaction [51,56,57]:

$$2NO_2(N_2O_4) \rightarrow NO_3{}^- + NO^+ \quad (6)$$

The nitrosonium ion, NO^+, chemisorbed on titania (anatase) and monoclinic zirconia gives rise to absorption band at 2206–2210 cm^{-1} [44,46,56–59].

The low intensity of the band attributed to the NO^+ species adsorbed on the ZrO_2 sample used in this study leads to the conclusion that the surface nitrates are obtained mainly by disproportionation of NO_2 with the involvement of the isolated hydroxyls at 3740 and 3693 cm^{-1} (reaction (5)).

The spectrum of NO and O_2 coadsorbed on the WZ sample (Fig. 6A) displays similar features to those of impregnated WO_3/ZrO_2 [47]. The strong bands in the 1650–1200 cm^{-1} region correspond to surface nitrates. The band at 1747 cm^{-1} is due to adsorbed N_2O_4, whereas the intense absorption at 2175 cm^{-1} corresponds to adsorbed NO^+ species [47]. The unresolved absorption at about 1930 cm^{-1} is assigned to Zr^{4+}–NO nitrosyl that has nitrate ions in its vicinity [47].

Compared to zirconia, the amounts of the gaseous species (Fig. 6B) and NO_x complexes adsorbed on the WZ sample (Fig. 6A) are greater. This fact indicates that the Brønsted acidity favors the oxidation of NO to NO_2, which is in agreement with the results of other reports [8,10]. The intense band due to adsorbed NO^+ species reveals the occurrence of surface reaction (6). Another possibility for the formation of nitrosonium ion is the reaction of NO and NO_2 with the Brønsted acid sites of tungstated zirconia via process observed to take place on acidic zeolites [60]:

$$NO + NO_2 + 2H^+ \rightleftharpoons H_2O + 2NO^+ \quad (7)$$

The water produced in this process can perturb the isolated hydroxyls (negative bands at 3740 and 3670 cm^{-1}) by H-bonding leading to appearance of positive absorption that extends below 3000 cm^{-1}. The possibility for involvement of the Brønsted acid sites of the tungstated zirconia in the formation of NO^+ species is supported by the fact that the replacement of protons of the surface hydroxyls (isolated and H-bonded) by Pd^{2+} ions causes significant decrease in the intensity of the NO^+ band detected under the same conditions (see below). It should be pointed out that we cannot discriminate between the perturbation of the Zr^{4+}–OH groups on tungstated zirconia due to their involvement in the NO_2 disproportionation according reaction (5) and the perturbation caused by the water molecules produced in reaction (7).

The weakly adsorbed species on the surface of the WZ sample, which disappear after evacuation at room temperature (Fig. 7, spectrum WZ), are identified as N_2O_4 (1747 cm^{-1}), NO_2 (~1620 cm^{-1}), Zr^{4+}–NO (~1930 cm^{-1}) and nitrate species most probably monodentate (1580 and 1278 cm^{-1}). The intensity of the NO^+ band decreases significantly, which is accompanied by lowering of the intensities of the negative band at 3670 cm^{-1} and the positive absorption in the region of H-bonded hydroxyls. This behavior can be explained assuming that nitrosonium ions are formed by reaction (7) and during the dynamic evacuation the reverse of the reaction is favored. Most probably the negative band at 3670 cm^{-1} belongs to W–OH groups. Recombination of NO^+ and $NO_3{}^-$ species to N_2O_4 during the evacuation can also contribute to the decrease in the amount of adsorbed NO^+ ions. The bands at 2604, 1975, 1905 and 1760 cm^{-1}, observed under these conditions are due to combination modes of the nitrate species [44]. The pair of bands at 1975 and 1905 cm^{-1} reveals the presence of bridged $NO_3{}^-$ species and corresponds to the split $\nu_s(NO_2) + \delta(ONO)$ mode, whereas the bands at 2604 ($\nu(NO) + \nu_s(NO_2)$ mode) and 1760 cm^{-1} (high-frequency component of the split $\nu_s(NO_2) + \delta(ONO)$ mode) belong to bidentate nitrates.

In contrast to the zirconia and WZ samples, the amount of NO_x species on the Pd/WZ is considerably lower (Fig. 6A). The gas phase spectrum (Fig. 6B) is identical to that recorded in the presence of zirconia, which indicates that the promotion of tungstated zirconia with palladium(II) suppresses the oxidation of NO by molecular oxygen at room temperature. This suppression is caused by the elimination of acidic protons involved in the NO oxidation. Formation of NO_2 during the catalytic reduction of NO with methane is considered to be an important step in the reaction mechanism [8–10,15,23,39]. We are of the opinion that the ability of Pd^{2+} ions to oxidize NO to NO_2 at high temperatures (shown above) could ensure sufficient amount of NO_2 under the reaction conditions despite the decrease in the Brønsted acidity. Reduction of Pd^{2+} in Pd-H-ZSM-5 to Pd^+ ions upon exposure to NO leading to formation of NO_2 was observed by Descorme et al. [3] using IR spectroscopy and in the XAFS measurements of Okumura et al. [19].

The fact that the hydroxyl content of the Pd/WZ sample is very low (see Fig. 3A) suggests that the nitrates species (bands in the 1650–1400 and 1300–1200 cm^{-1} regions) are produced mainly via reaction (6). The broad absorption with maximum at 2160 cm^{-1} is due to the ν(NO) stretching mode of the NO^+ species. The intensity of this band is much lower than that on the WZ sample. The Pd^{2+}–NO nitrosyls give rise to the bands at

1870 and 1820 cm^{-1}, whereas the adsorbed N_2O_4 produces the band at 1748 cm^{-1} (ν_{as}(NO) mode). The prolonged evacuation (for 30 min) at room temperature (Fig. 7, spectrum Pd/WZ) leads to decrease in the intensity of the former two bands and disappearance of the adsorbed N_2O_4. In contrast to the WZ sample, the NO^+ species on Pd/WZ resist the room temperature evacuation. The stability of the NO^+ species can be associated with the decrease in the amount of Brønsted acid sites.

The negative band at 1012 cm^{-1} observed on both WZ and Pd/WZ samples (Figs. 6A and 7) indicates perturbation of the W=O species. The band at 1037 cm^{-1}, which is offset by the negative absorption at 1012 cm^{-1}, is due to the $\nu_s(NO_2)$ modes of the nitrate species.

The thermal stability of the strongly bound NO_x species formed by room-temperature NO/O_2 coadsorption has been examined under dynamic evacuation at elevated temperatures. The surface nitrates adsorbed on zirconia disappear after heating at 723 K. The nitrates formed on the WZ and Pd/WZ samples have comparable thermal stability: they are removed at 673 K.

4. Conclusions

Mesoporous tungstated zirconia prepared by coprecipitation of aqueous solutions of $ZrOCl_2{\cdot}8H_2O$ and ammonium metatungstate possesses the ability to stabilize dispersed Pd(II) species in two different environments: (i) Pd^{2+} ions, which have only Zr^{4+} ions in their second coordination sphere and (ii) Pd^{2+} ions, which are attached to both zirconium and tungsten ions via oxygen bridges.

Depending on the temperature, NO can be oxidized in the presence of Pd/WZ sample to various NO_x species. The compounds formed at room-temperature oxidation are adsorbed N_2O_3 and products of its self-ionization, NO^+ and NO_2^-. In this process W(VI) is involved, being reduced to W(IV). At high temperature N_2O_3 decomposes, restoring the W=O species. Under these conditions, NO undergoes oxidation to NO_2 by the Pd(II) ions, which are reduced to Pd(I). The nitrosyls of Pd(I) display high thermal stability and do not disappear upon evacuation at 623 K.

During NO/O_2 coadsorption on the Pd/WZ catalyst at room temperature, the amounts of surface nitrates and NO_2/N_2O_4 formed in the gas phase are significantly lower than those observed under identical conditions in the presence of tungstated zirconia. It is concluded that promotion of tungstated zirconia with palladium(II) suppresses the oxidation of NO by molecular oxygen at room temperature. This effect is due to the elimination of acidic protons involved in the process. The thermal stability of the NO_3^- species adsorbed on the WZ and Pd/WZ samples is comparable, although lower than that in the case of zirconia.

Acknowledgment

This work was financially supported by Bilkent University and the Scientific and Technical Research Council of Turkey (TÜBITAK), Project TBAG-2140.

References

[1] Y. Li, J.N. Armor, Appl. Catal. B: Environ. 1 (1992) L31.
[2] Y. Traa, B. Burger, J. Weitkamp, Micropor. Mesopor. Mater. 30 (1999) 3.
[3] C. Descorme, M. Gélin, M. Primet, C. Lécuyer, Catal. Lett. 41 (1996) 133.
[4] C. Descorme, M. Gélin, C. Lécuyer, M. Primet, Appl. Catal. B: Environ. 41 (1996) 133.
[5] C. Descorme, M. Gélin, C. Lécuyer, M. Primet, J. Catal. 177 (1998) 352.
[6] H. Ohtsuka, T. Tabata, Appl. Catal. B: Environ. 21 (1999) 133.
[7] C.M. Correa, F. Cordoba, F. Bustamente, Micropor. Mesopor. Mater. 40 (2000) 149.
[8] Y. Nishizaka, M. Misono, Chem. Lett. (1993) 1295.
[9] Y. Nishizaka, M. Misono, Chem. Lett. (1994) 2237.
[10] C.J. Loughran, D.E. Resasco, Appl. Catal. B: Environ. 113 (1995) 351.
[11] A. Ali, W. Alvarez, C.J. Loghran, D.E. Resasco, Appl. Catal. B: Environ. 14 (1997) 13.
[12] A. Ali, Y.H. Chin, D.E. Resasco, Catal. Lett. 56 (1998) 111.
[13] B.J. Adelman, W.M.H. Sachtler, Appl. Catal. B: Environ. 14 (1997) 1.
[14] M. Ogura, M. Hayashi, S. Kage, M. Matsukata, E. Kikuchi, Appl. Catal. B: Environ. 23 (1999) 247.
[15] G. Koyano, S. Yokoyama, M. Misono, Appl. Catal. A: Gen. 188 (1999) 301.
[16] A.W. Aylor, L.J. Lobree, J.A. Reimer, A.T. Bell, J. Catal. 172 (1997) 453.
[17] L.J. Lobree, A.W. Aylor, J.A. Reimer, A.T. Bell, J. Catal. 181 (1999) 189.
[18] K. Okumura, J. Amano, M. Niwa, Chem. Lett. (1999) 997.
[19] K. Okumura, J. Amano, N. Yasunobu, M. Niwa, J. Phys. Chem. B 104 (2000) 1050.
[20] K. Okumura, M. Niwa, Catal. Surv. Jpn. 5 (2002) 121.
[21] Y.H. Chin, A. Pisanu, W.A. Serventi, W.E. Alvarez, D.E. Resasco, Catal. Today 54 (1999) 419.
[22] Y.H. Chin, W.E. Alvarez, D.E. Resasco, Catal. Today 62 (1999) 159.
[23] Y.H. Chin, W.E. Alvarez, D.E. Resasco, Catal. Today 62 (1999) 291.
[24] K. Okumura, T. Kusakabe, M. Niwa, Appl. Catal. B: Environ. 41 (2003) 137.
[25] D.G. Barton, S.L. Soled, E. Iglesia, Top. Catal. 6 (1998) 87.
[26] E. Iglesia, D.G. Barton, S.L. Soled, S. Mieso, J.E. Baumgartner, W.E. Gates, G.A. Fuentes, G.D. Meitzner, in: J.W. Hightower, W.N. Delgass, E. Iglesia, A.T. Bell (Eds.), Studies in Surface Science and Catalysis, vol. 101, Elsevier, Amsterdam, 1996, p. 533.
[27] D.G. Barton, M. Shtein, R.D. Wilson, S.L. Soled, E. Iglesia, J. Phys. Chem. B: Environ. 103 (1999) 630.
[28] M. Scheithauer, R.K. Grasselli, H. Knözinger, Langmuir 14 (1998) 3019.
[29] M. Hino, K. Arata, J. Chem. Soc., Chem. Commun. (1987) 1259.
[30] J.G. Santiesteban, J.C. Vartuli, S. Han, R.D. Bastian, C.D. Chang, J. Catal. 168 (1997) 431.
[31] P. Vijayanand, K. Chakarova, K. Hadjiivanov, P. Likinskas, H. Knözinger, Phys. Chem. Chem. Phys. 5 (2003) 4040.
[32] O.V. Melezhyk, S.V. Prudis, V.V. Brei, Micropor. Mesopor. Mater. 49 (2001) 39.
[33] C.E. Crouthamel, C.E. Johnson, Anal. Chem. 26 (1954) 1284.
[34] D.F. Wood, R.T. Clark, Analyst 83 (1958) 326.
[35] Y.-C. Xie, Y.-Q. Tang, Adv. Catal. 37 (1997) 1.
[36] M.P. Klug, L.E. Alexander, X-ray Diffraction Procedure for Polycrystalline and Amorphous Materials, Wiley, New York, 1974, p. 634.
[37] M. Kang, D. Kim, S.H. Yi, J.U. Han, J.E. Yie, J.M. Kim, Catal. Today 93–95 (2004) 695.
[38] A. Rakai, D. Tessier, F. Bozon-Verduraz, New J. Chem. 16 (1992) 869.
[39] K. Shimizu, F. Okada, Y. Nakamura, A. Satsuma, T. Hattori, J. Catal. 195 (2000) 151.
[40] K.T. Jung, A.T. Bell, J. Mol. Catal. A: Chem. 163 (2000) 27.
[41] A. Gutierrez-Alejandre, P. Castillo, J. Ramirez, G. Ramis, G. Busca, Appl. Catal. A: Gen. 216 (2001) 181.

[42] M. Scheithauer, T.-K. Cheung, R.E. Jentoft, R.K. Grasselli, B.C. Gates, H. Knözinger, J. Catal. 180 (1998) 1.
[43] S. Triwahyono, T. Yamada, H. Hattori, Appl. Catal. A: Gen. 250 (2003) 75.
[44] M. Kantcheva, E.Z. Ciftlikli, J. Phys. Chem. B 106 (2002) 3941.
[45] K.I. Hadjiivanov, Catal. Rev.-Sci. Eng. 42 (2000) 71.
[46] K. Hadjiivanov, V. Avreyska, D. Klissurski, T.S. Marinova, Langmuir 18 (2000) 1619.
[47] T. Weingand, S. Kuba, K. Hadjiivanov, H. Knözinger, J. Catal. 209 (2002) 539.
[48] D. Onafi, F. Mauge, J.-C. Lavalley, Bull. Soc. Chim. Fr. (1989) 363.
[49] Y. Yan, Q. Xin, S. Jiang, X. Guo, J. Catal. 131 (1991) 234.
[50] K. Hadjiivanov, P. Lukinskas, H. Knözinger, Catal. Lett. 82 (2002) 73.
[51] E. Ito, Y.J. Mergler, B.E. Nieuwenhuys, H. van Bekkum, C.M. Van den Bleek, Micropor. Mater. 4 (1995) 455.
[52] S.-J. Huang, A.B. Walters, M.A. Vannice, J. Catal. 192 (2000) 29.
[53] J. Laane, J.R. Ohlsen, Prog. Inorg. Chem. 28 (1968) 465.
[54] N. Mcleod, R. Cropley, R.M. Lambert, Catal. Lett. 86 (2003) 69.
[55] A.F. Holleman, E. Wiberg, Inorganic Chemistry, Academic Press, 2000, p. 653.
[56] M.M. Kantcheva, V.P. Bushev, K.I. Hadjiivanov, J. Chem. Soc., Faraday Trans. 88 (1992) 3087.
[57] K. Hadjiivanov, V. Bushev, M. Kantcheva, D. Klissurski, Langmuir 10 (1994) 464.
[58] M. Kantcheva, J. Catal. 204 (2001) 479.
[59] K. Hadjiivanov, H. Knozinger, Phys. Chem. Chem. Phys. 2 (2000) 2803.
[60] K. Hadjiivanov, J. Saussey, J.L. Freysz, J.C. Lavalley, Catal. Lett. 52 (1998) 103.